Shock Waves (2003) 13: 113–121
Digital Object Identifier (DOI) 10.1007/s00193-003-0198-x

Shock Waves

Effect of energy addition on MR → RR transition

H. Yan[1], R. Adelgren[2], G. Elliott[3], D. Knight[1], T. Beutner[4]

[1] Dept. of Mechanical and Aerospace Engineering, Rutgers – The State University of New Jersey, Piscataway, NJ 08854, USA
[2] USAF Test Pilot School, Edwards Air Force Base, CA 93524, USA
[3] Dept. of Aeronautical and Astronautical Engineering, University of Illinois Urbana Champaign, Urbana, IL 61801, USA
[4] Air Force Office of Scientific Research, 801 N. Randolph St., Arlington, VA 22203, USA

Received 27 February 2003 / Accepted 3 June 2003
Published online 11 July 2003 – © Springer-Verlag 2003
Communicated by H. Grönig

Abstract. A combined computational and experimental study was performed to investigate the effect of a single laser energy pulse on the transition from a Mach Reflection (MR) to a Regular Reflection (RR) in the Dual Solution Domain (DSD). The freestream Mach number is 3.45 and two oblique shock waves are formed by two symmetric 22° wedges. These conditions correspond to a point midway within the DSD wherein either an MR or an RR is possible. A steady MR was first obtained experimentally and numerically, then a single laser pulse was deposited above the horizontal center plane. In the experiment, the laser beam was focused resulting in a deposition volume of approximately 3 mm^3, while in the simulation, the laser pulse was modeled as an initial variation of the temperature and pressure using Gaussian profile. A grid refinement study was conducted to assess the accuracy of the numerical simulations. For the steady MR, the simulation showed the variation of Mach stem height along the span due to side effects. The predicted spanwise averaged Mach stem height was 1.96 mm within 2% of the experimental value of 2 mm. The experiment showed that the Mach stem height decreased to 30% of its original height due to the interaction with the thermal spot generated by the laser pulse and then returned to its original height by 300 μs. That the Mach stem returned to its original height was most likely due to freestream turbulence in the wind tunnel. The numerical simulation successfully predicted the reverse transition from a stable MR to a stable RR and the stable RR persisted across the span. This study showed the capability of a laser energy pulse to control the reverse transition of MR → RR within the Dual Solution Domain.

Key words: Local flow control, MR → RR transition, Laser pulse

1 Introduction

Aerodynamic flow control has an important impact on the design of high performance supersonic and hypersonic air vehicles. Knight et al. (2002) recently surveyed research efforts on aerodynamics of flow control using energy deposition. A great effort (Chernity 1999; Levin and Terent'eva 1993; Myrabo and Raizer 1994; Pilyugin et al. 1997; Riggins et al. 1999; Toro et al. 1998; Tretyakov et al. 1996) has been focused on *global* flow control using energy deposition for drag reduction and modification of vehicle aerodynamic forces and moments, and MHD control. More recently, attention has been directed towards *local* flow control due to the highly localized fluid dynamic phenomena involved with the aerodynamic performance, *e.g.*, reducing peak surface pressure and heat transfer, modifying separation regions, changing the shock structure, *etc*. As opposed to *global* flow control, *local* flow control requires only small scale energy addition.

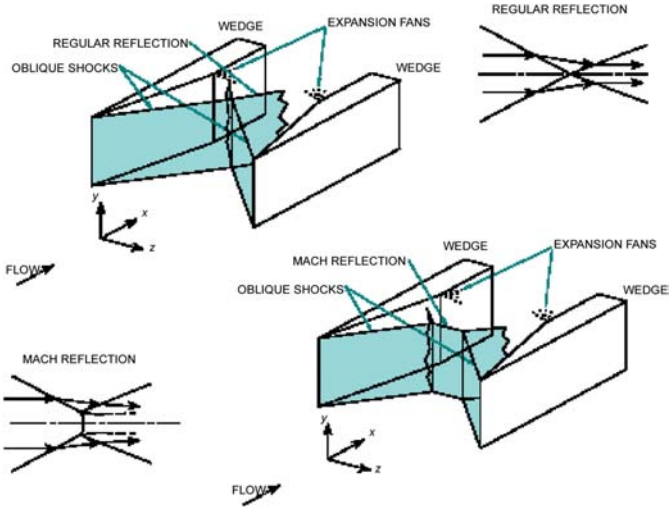

Fig. 1. MR and RR

Correspondence to: H. Yan (e-mail: honyan@jove.rutgers.edu)

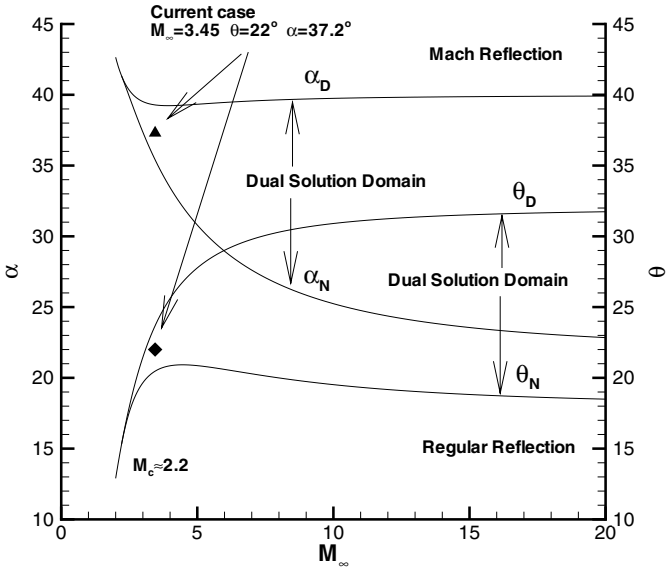

Fig. 2. Dual solution domain

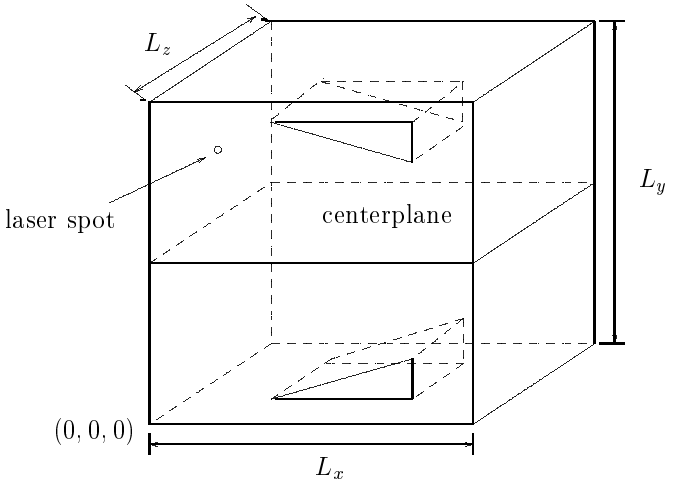

Fig. 3. Computational domain

The crossing shock wave interaction is a fundamental phenomenon in high speed flight. For example, a scramjet powered hypersonic vehicle may utilize shock interactions to decelerate the flowfield in the inlets for more efficient combustion. The intersection of two symmetric oblique shock waves may result in either an RR or an MR (Fig. 1). When the incoming Mach number (M_∞) exceeds a critical Mach number M_C (where M_C is 2.202 for a diatomic gas (Molder 1979) and is approximately 2.2 for perfect air), a Dual Solution Domain (DSD) is formed, wherein either an RR or an MR can theoretically exist. The DSD is bounded by the detachment angle α_D and the von Neumann angle α_N as illustrated in Fig. 2, wherein α is the shock angle and θ is the wedge angle. Two conditions for the RR ↔ MR transition are the detachment condition (α_D) beyond which an RR wave configuration is theoretically impossible and the von Neumann condition (α_N) below which an MR wave configuration is theoretically impossible. Von Neumann (1963) was the first to introduce these two conditions as possible RR ↔ MR transition criteria.

Hornung et al. (1979) hypothesized that a hysteresis could exist within the DSD. For increasing α (beginning with $\alpha < \alpha_N$, *i.e.*, an RR), the forward transition angle α^F_{tr} for RR → MR equals α_D. For decreasing α (beginning with $\alpha > \alpha_D$, *i.e.*, an MR), the backwards transition angle for MR → RR equals α_N. Experiments and numerical simulations by Chpoun et al. (1994) and Ivanov et al. (1995), (1996), (1997), (1998), (2001) confirmed the hysteresis model of Hornung et al. (1979). A recent review paper by Ben-Dor et al. (2002) summarized the recent research on hysteresis induced by the Mach number variation and the wedge angle variation. This paper also discussed the influence of three dimensional effects and freestream perturbations on the RR ↔ MR transition. Chpoun et al. (1995) experimentally suggested that the three dimensional effects have a larger influence on the RR → MR transition than on the $MR \rightarrow RR$ transition. Many other researchers (Ivanov et al. 1997; Schmisseur and Gaitonde 2001; Skews 1997, 2000) also claimed that their experimental results were affected by three-dimensional edge effects. Ivanov et al. (1996) and Khotyanovsky et al. (1999) investigated the influence of freestream density perturbations on the RR ↔ MR transition. They proposed the threshold level of the perturbations capable of causing such transition.

In the DSD, either an RR or an MR is theoretically possible. Different shock structures may significantly affect the entire performance of the vehicle. For example, at Mach 5 and $\alpha = 35°$ (*i.e.*, midway between α_N and α_D), the stagnation pressure ratio across the RR is 349% greater than the MR. Consequently, the ability to control the RR ↔ MR transition is important for scramjet propulsion. The intersecting oblique shock waves may be viewed as representative of a high speed inlet, wherein the appearance of an MR causes a significant degradation in propulsion efficiency due to the decreased total pressure recovery compared to an RR. Assuming the inlet design point lies below the von Neumann angle (*i.e.*, the inlet is designed for an RR only), it is nonetheless possible for the inlet to momentarily be in the DSD (due to vehicle maneuver or gust response) wherein an RR → MR transition can spontaneously occur.

The objective of this combined computational and experimental study is to determine the capability of laser energy deposition to momentarily reduce the extent of the Mach stem or even to force a transition from a stable MR to a stable RR within the Dual Solution Domain, thereby improving total pressure recovery and propulsion efficiency.

2 Flow configuration

A Mach 3.45 flow enters two symmetric 22° wedges, which corresponds to a point midway in the DSD shown in Fig. 2. Once an MR is formed, a single laser pulse (E =215 mJ) is added above the horizontal center plane and on the vertical center plane shown in the numerical model (Fig. 3).

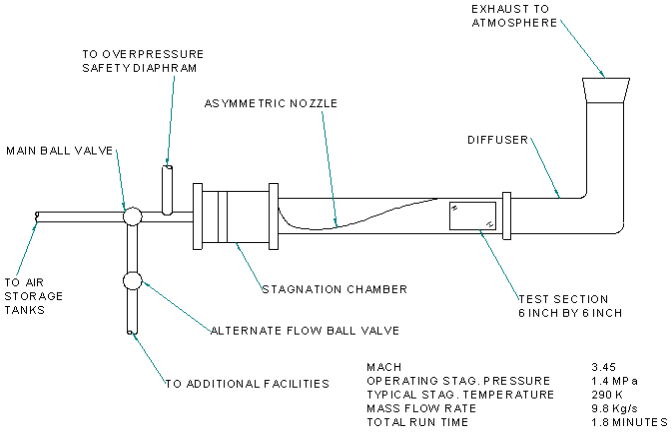

Fig. 4. Schematic of Rutgers supersonic wind tunnel

Table 1. Test conditions and model dimensions

c_v (m^2/s^2K)	E (J)	$p_{t\infty}$ (MPa)	T_{t_∞} (K)	V_0 (mm^3)	ρ_∞ (kg/m^3)
717.5	0.215	1.138	283	3	0.667
θ (deg)	α (deg)	α_D (deg)	α_N (deg)		
22	37.3	39.3	35.4		
w (mm)	b/w	$2g/w$	M_∞		
25.4	2.198	1.19	3.45		

Legend

θ	wedge angle	α	shock angle (theory)
w	shock generator length		
b	total spanwise length	$2g$	wedge separation distance

3 Experimental facilities

All experiments were performed in the Mach 3.45 supersonic wind tunnel of the Rutgers Gas Dynamics and Laser Diagnostics Laboratory (Fig. 4). The tunnel is a blow-down facility with compressed air supplied from high pressure (16.6 MPa) air storage tanks with a capacity of 8 m^3. Three four-stage compressors and a regenerative air dryer are employed. The test section is 15.2 cm × 15.2 cm, and the total available test time is several minutes per day. Test section stagnation pressure can be set in the range of 0.55 to 4.8 MPa, with a typical value of 1.0 MPa, and the stagnation temperature is ambient (typically 290 K). The Reynolds number per meter is $1.5 - 24.0 \times 10^7$.

A short duration (10 ns) laser pulse is generated using a frequency doubled Nd:YAG laser (wavelength $\lambda = 532$ nm). The laser beam (1 cm diameter) is focused through a lens (typically 100 mm focal length) to a small volume (resulting in an energy deposition region of 3 mm^3). The incident beam energy for the experiments described herein is 215 mJ (measured before the focusing lens) and the laser pulse repetition rate is 10 Hz. Additional information is presented in Adelgren et al. (2001).

Schlieren visualization is performed using a xenon flashlamp with 1 μs pulse duration. The schlieren image is captured on a CCD camera and digitized. At typical tunnel stagnation conditions, the freestream velocity is 640 m/s, yielding an effective flow transit distance of 0.64 mm during the schlieren pulse. A typical model dimension (in the cross sectional plane) is 25.4 mm. Thus, the schlieren image is effectively instantaneous; however, the image is optically integrated in the spanwise direction due to the inherent nature of schlieren. Typically multiple images are ensemble averaged at the same time delay following the laser pulse.

The test conditions and dimensions of the wedge model are shown in Table 1, where p_t and T_t are stagnation pressure and temperature, respectively, and the subscript ∞ denotes the freestream condition.

4 Numerical methodology

The computational domain $L_x \times L_y \times L_z$ shown in Fig. 3 is $3.5w \times 4w \times 2.2w$, where $w = 25.4$ mm is the shock generator length measured along wedge surface. The $x = 0$, $y = 0$ and $z = 0$ planes are the inflow boundary, the lower boundary and the vertical centerplane, respectively. The streamwise length L_x was chosen to insure supersonic flow at the downstream boundary and to keep the blast wave from the laser pulse away from the upstream boundary. The transverse and spanwise lengths L_y and L_z are based on the requirement that the reflections at the boundaries of the acoustic disturbances originating from the tip of the wedge and the blast waves from the laser pulse do not interact with the flow structure in the vicinity of the Mach stem. The trailing edges of the two wedges are placed $2.5w$ downstream of the inflow. The center of the laser spot is located at $0.2w$ downstream of the leading edge and $0.9w$ above the horizontal center plane in accordance with the experiment.

The flow solver is GASPex which solves the compressible Euler equations. The third-order accurate Van Leer scheme along with Mid-Mod limiter is used to compute the inviscid fluxes in each direction and a two-stage Runge-Kutta scheme is used for the time integration.

The inflow boundary is a uniform Mach 3.45 flowfield and the extrapolation technique is used for the outflow. The symmetric boundary is used for the $z = 0$ plane. The slip boundary condition is utilized on the wedge surfaces and also on the upper and lower boundary and $z = L_z$ plane for simulating the wind tunnel side walls.

The grid is generated by a commercial software ICEM-CFD. Two sets of grids are generated to conduct a grid refinement study. Approximately 11 to 25 layers of cells are used to resolve the Mach stem in the vertical direction for the coarse and fine grids, respectively. The total number of cells are 1.5 million and 5.0 million for the coarse and fine grids, respectively. The grid convergency is demonstrated in Fig. 5.

The laser energy addition is modeled as a temperature variation and the breakdown of air is not considered.

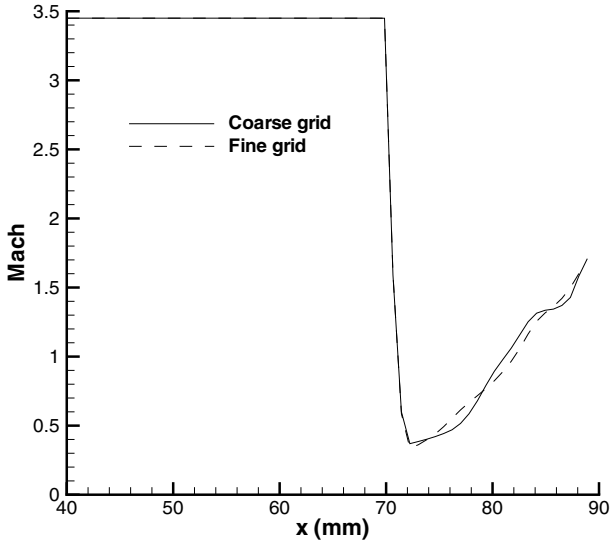

Fig. 5. Mach number along centerline

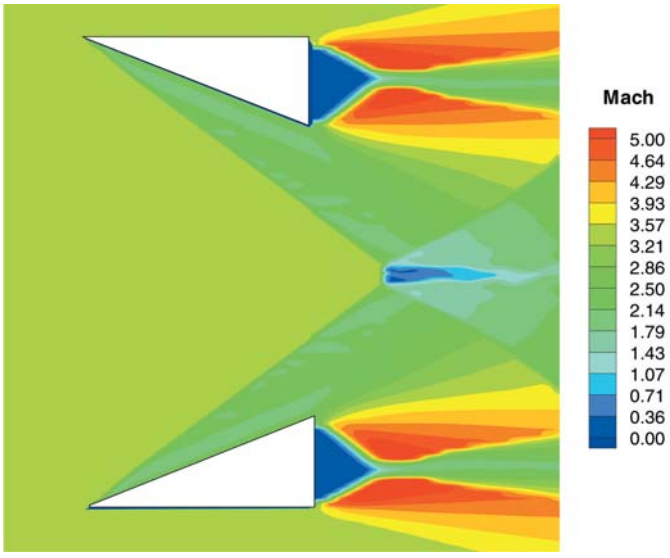

Fig. 6. Mach number contours at vertical centerplane

The details are presented in Yan et al. (2003). The initial condition for no energy addition is

$$\begin{aligned} \rho &= \rho_\infty \\ u &= 0.5 \times M_\infty a_\infty \\ v &= 0 \\ w &= 0 \\ T &= T_\infty \ . \end{aligned} \tag{1}$$

5 Results

The computation is performed in two steps. The flowfield is first converged to a steady state in the absence of any laser perturbation. Then a laser pulse is added by simulating an initial Gaussian temperature distribution at a specific location.

The steady flow structure without the energy perturbation is first shown. The steady state is obtained when the Mach stem location doesn't change with time at the vertical centerplane. Figure 6 demonstrates the flow structures at the $z = 0$ plane for the fine grid. Two oblique shock waves generated by the leading edges form a Mach reflection. The flow after this normal shock becomes subsonic. The expansion fans emanating from the trailing edges are refracted through the reflected shocks and interact with slipstreams, forming a converging-diverging nozzle to accelerate the flow to be supersonic. The Kelvin-Helmholtz structures are clearly observed propagating along the sliplines, due to the difference in both the velocity and the density along the sliplines. The predicted spanwise averaged Mach stem height is 1.96 mm for the coarse and fine grid, and it is within 2% of the experimental value of 2 mm. The measurement uncertainty of the Mach stem height is ±10%. All the following computational results are shown for the fine grid simulation.

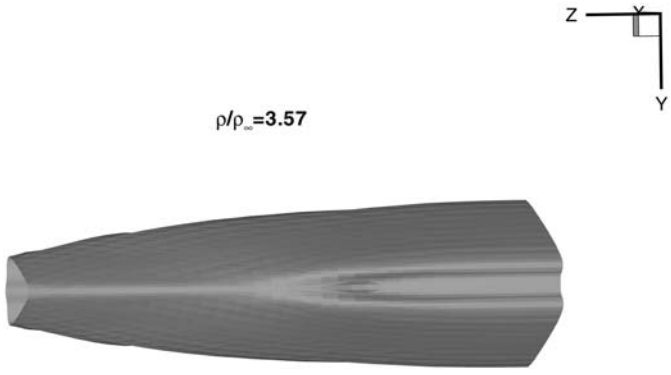

Fig. 7. Density isosurface for MR

Three dimensional effects, due to the finite aspect ratio of the wedges, are seen in the spanwise variation of the Mach stem height. Figure 7 shows this variation in a plot of the isosurface of density for $\rho/\rho_\infty = 3.57$. The Mach stem decreases in height from the centerplane (which corresponds to the right edge in the figure) and disappears close to the edge of the wedge (which corresponds to the left edge in the figure). This observation is consistent with the study by Ivanov et al. (2001).

Once the steady MR is formed, a laser pulse is added. The experimental schlieren images are shown in Figs. 8 in which each experimental schlieren image is an ensemble of three to eight experiments, although the instantaneous images show the same trends as described below. The numerical schlieren images which are the contour plot of the first derivative of the density along the streamwise direction at the $z = 0$ plane are plotted for qualitative comparison in Figs. 9.

Figures 8a to 8b and Figs. 9a to 9b show the process of the blast wave and the thermal spot interacting with the upper oblique shock wave, causing an upstream deflection of the oblique shock due to the lowering of the local

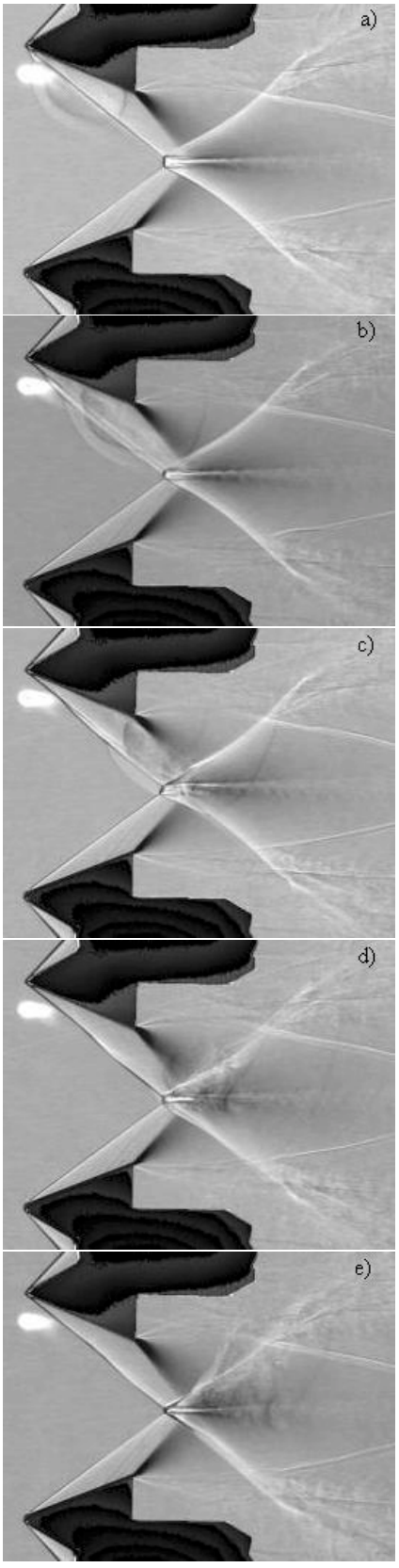

Fig. 8a–e. Experiment, **a** $t = 20$ µs, **b** $t = 40$ µs, **c** $t = 60$ µs, **d** $t = 80$ µs, **e** $t = 100$ µs

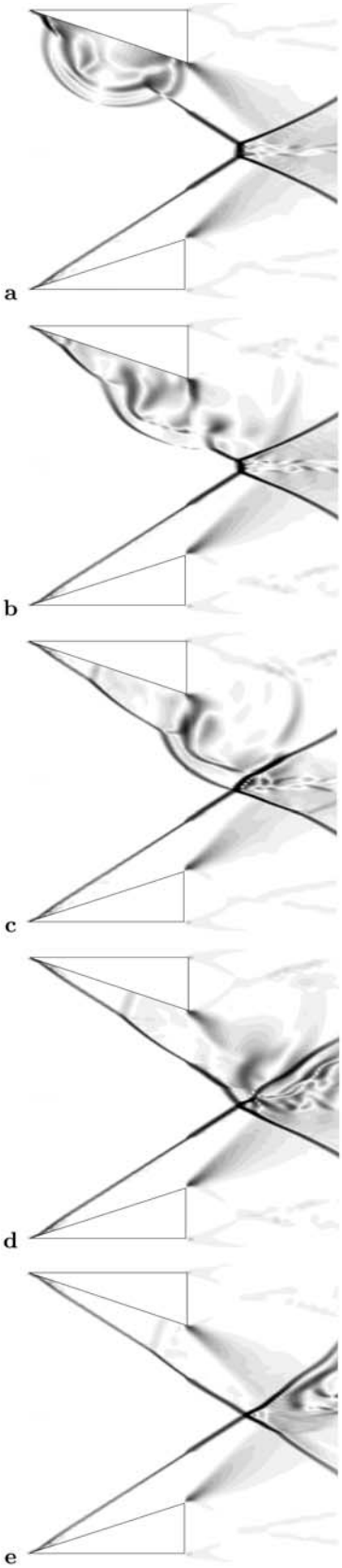

Fig. 9a–e. Simulation, see Fig. 8 for legend

Mach number from the thermal spot. This deflection eventually reaches the Mach stem (Figs. 8c and 9c) at approximately $t = 60$ μs causing a reduction in the height of the Mach stem. In the experiment, the Mach stem decreases monotonically to 30% of its original height as shown in Fig. 10. This return to an MR may be due to freestream disturbances in the tunnel. The simulation shows that the Mach stem finally disappears along the entire wedge span as shown in Fig. 11 and Fig. 12 and a complete transition of MR to RR is achieved. The computation runs for 2.0 flowthrough times following the establishment of the RR (where, one flowthrough time is defined as the time for the freestream to traverse the whole computational domain) and the RR is stable as shown in Fig. 11 (where $t = 280$ μs is the limit of the computation).

Figures 13 and 14 show the pressure and Mach number contours at the vertical center plane at the corresponding experimental times. The blast wave formed by the energy deposition and rapid expansion of gas in the focal region propagates at supersonic speed relative to the thermal spot and an expansion fan is formed immediately behind the blast wave. From the previous study by Yan et al. (2003), the blast wave weakens very fast and essentially becomes an acoustic wave after $t = 10$ μs. A subsonic region formed due to the significant temperature increase in the focal region and the blast wave interact with the upper oblique shock, causing the stretching of the blast wave and the subsequent increase of its radius of curvature. Meanwhile the blast wave is reflected on the wedge surface shown in Fig. 13a, and the reflected blast wave cuts through the subsonic region seen in Fig. 14a. The thermal spot and the blast wave change the shock structures dramatically, not only at the centerplane, but also along the whole wedge span. Their effects on the shock structures are shown in Fig. 7 and Fig. 11. The same global effect of a small thermal spot on the shock structures was observed by Kolesnichenko et al. (2003), who investigated the interaction of the thin density wells with the supersonic blunt body.

The transition from an MR to an RR may be described as follows. As mentioned above, the thermal spot and its induced blast wave convect with the freestream, and first intersect with the upper oblique shock. Their intersections generate a complicated shock system, including the reflection of the blast wave and expansion waves on the wedge surface, and the deflection and lensing of the upper oblique shock (Adelgren 2002). As the deflected upper oblique shock reaches the Mach stem, the local shock angle is smaller than that for the lower oblique shock, therefore these symmetric double wedges actually act as two asymmetric wedges. Figure 2 shown for symmetric double wedges is not suitable to explain the transition any more. Li et al. (1999) and Ivanov et al. (2002) demonstrated that a hysteresis phenomenon existed in the reflection of asymmetric shock waves. Following this idea, we consider that the asymmetric laser pulse may affect the shock reflection from the symmetric reflection to the asymmetric reflection. Figure 15 shows the DSD in (θ_1, θ_2) plane for $M_\infty = 3.45$, where θ_1 and θ_2 denote the lower and upper

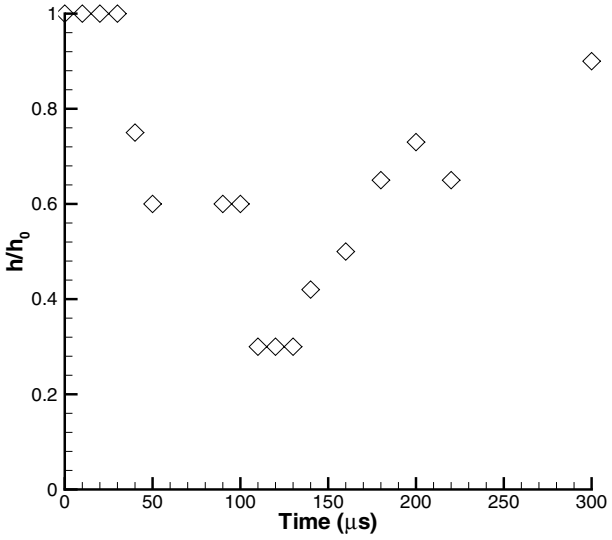

Fig. 10. Mach stem height *vs* t in experiment

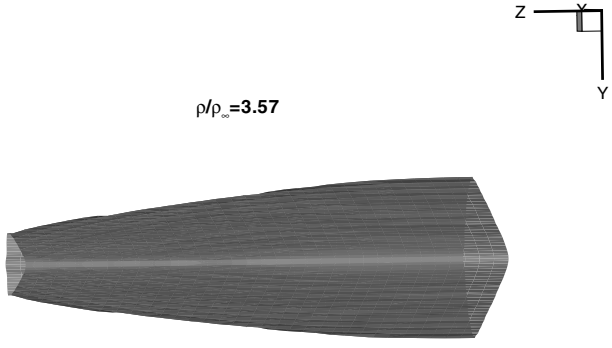

Fig. 11. Density isosurface at $t = 280$ μs

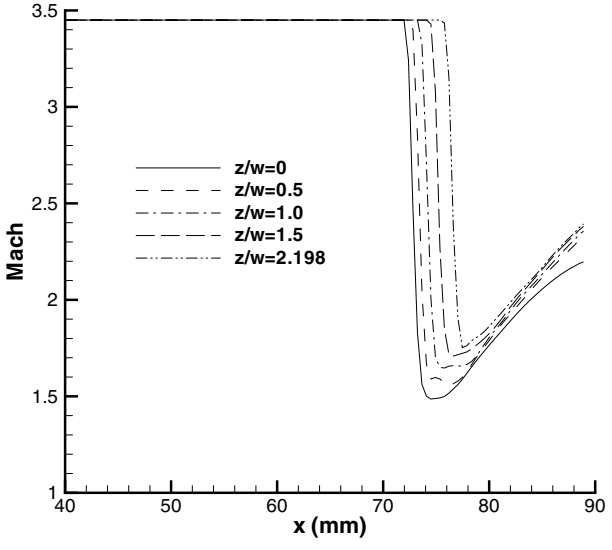

Fig. 12. Mach number along x at different span locations at $t = 280$ μs

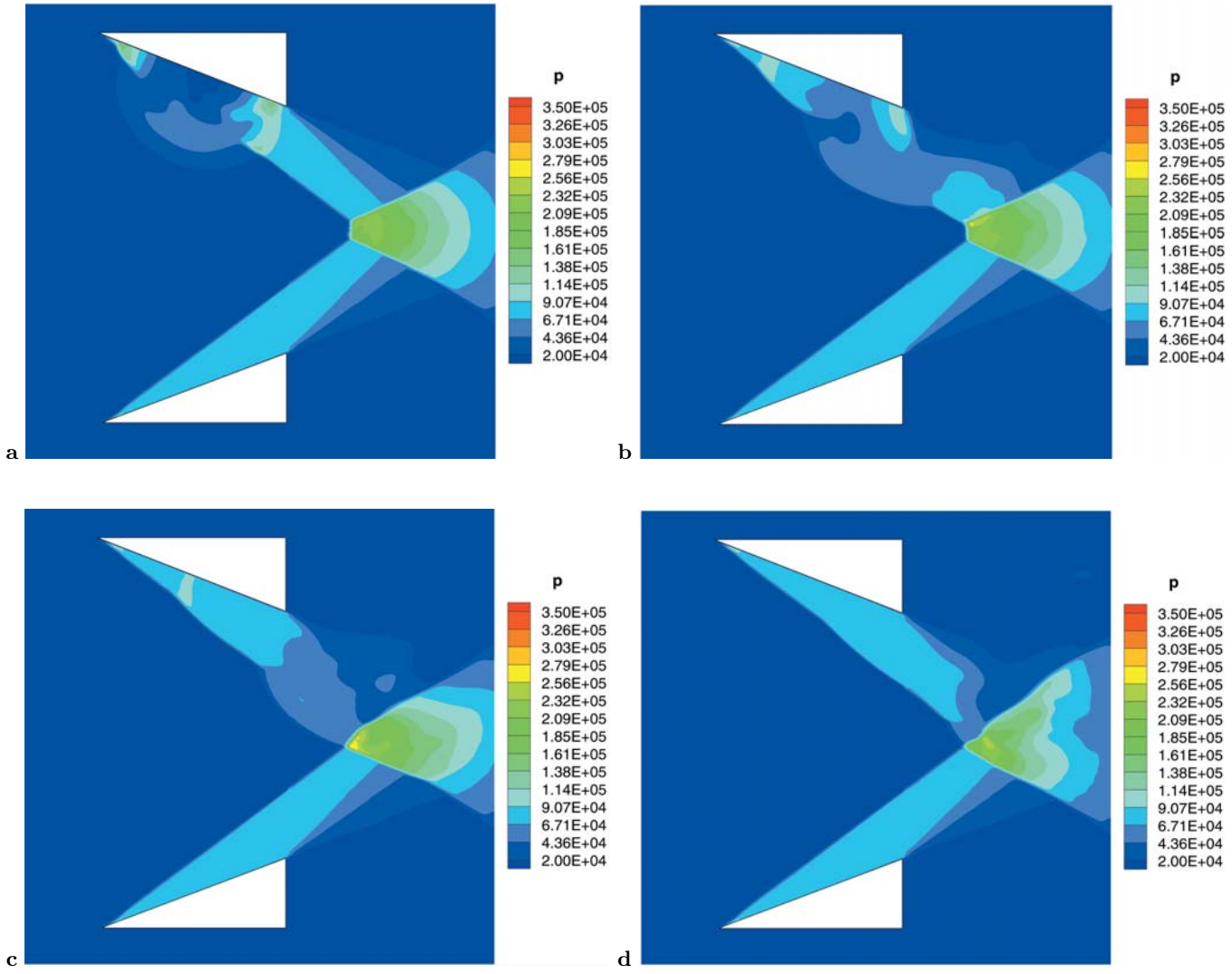

Fig. 13a–d. Pressure contours, **a** $t = 20$ µs, **b** $t = 40$ µs, **c** $t = 60$ µs, **d** $t = 80$ µs

wedge angle, respectively. The initial wedge angle is displayed by a diamond symbol in the middle of the DSD, and it is also plotted in (α_1, α_2) plane in Fig. 15, where α_1 and α_2 denote the lower and upper oblique shock angle, respectively. The MR → RR transition is described in Fig. 15. As the deflected upper oblique shock reaches the Mach stem, the local shock angle is decreased to approximately 11° as shown in Fig. 14c, while the lower oblique shock angle remains almost unchanged (37.3°). The initial point in the DSD moves below the von Neumann angle, wherein only an RR exists. When the thermal effects passes the Mach stem, the upper oblique shock angle changes back to its initial value into the DSD. However, the RR remains stable unless the shock angle reaches the detachment angle Hornung et al. (1979).

6 Conclusions

The paper presents a combined numerical and experimental study of intersecting shocks formed by 22° × 22° wedges at Mach number of 3.45 with a single asymmetric laser energy deposition. The shock wave angle is within the Dual Solution Domain wherein either a Mach Reflection or Regular Reflection is theoretically possible. In the absence of the laser energy deposition, the Mach Reflection is observed in both the experiment and simulation with the prediction of the Mach stem height in good agreement with the experiment. The 3D structure of the shock wave is shown in the simulation due to the finite width of the wedges. A laser energy pulse is added after the Mach reflection is established. In the experiment, the Mach stem is reduced to 30% of the original height and subsequently returns to its original height. A complete transition of MR → RR is obtained in the simulation. The study shows

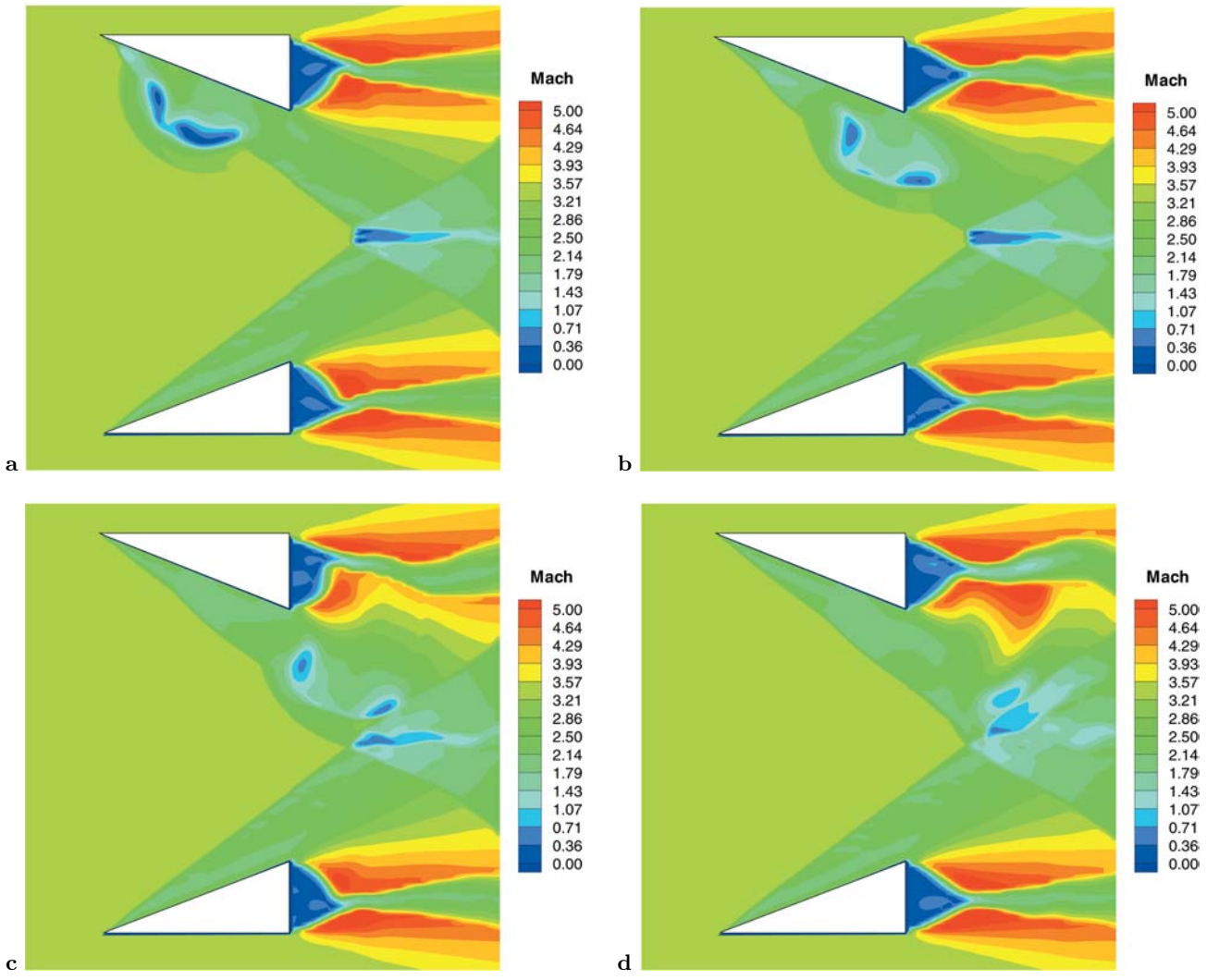

Fig. 14a–d. Mach number contours, **a** $t = 20$ μs, **b** $t = 40$ μs, **c** $t = 60$ μs, **b** $t = 80$ μs

the capability of a laser energy pulse to control the reverse transition of MR → RR.

Acknowledgements. This research is supported by Air Force Office of Scientific Research (AFOSR) under Grant No. F49620-01-1-0368 monitored by John Schmisseur and Steve Walker.

References

Adelgren R, Elliott G, Knight D, Ivanov M (2001) Preliminary Study of Localized Pulsed Laser Energy Deposition Effects on Shock Structures in Mach/Regular Reflection Dual Solution Domain at Mach 3.45. Report RU-TR-MAE-213, Dept of Mechanical and Aerospace Engineering, Rutgers University, July

Adelgren R (2002) Localized Flow Control with Energy Deposition. Ph.D dissertation, Dept of Mechanical and Aerospace Engineering, Rutgers University, September

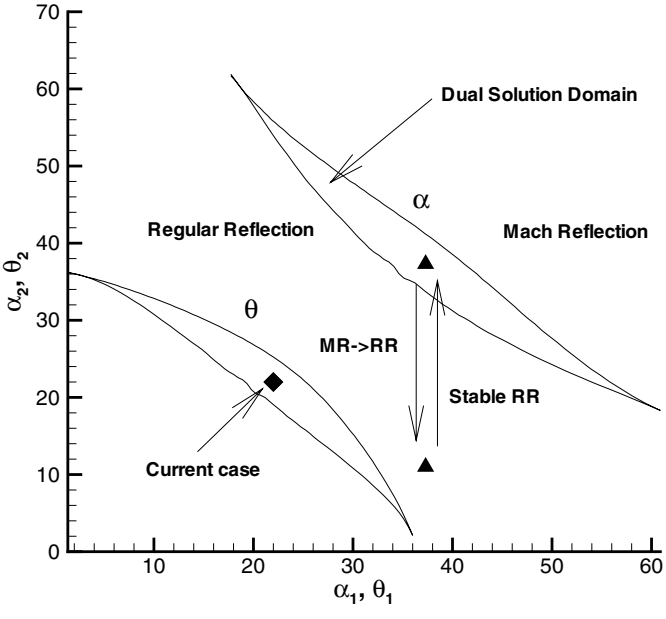

Fig. 15. (α_1, α_2) plane and (θ_1, θ_2) plane for $M_\infty = 3.45$

Ben-Dor G, Ivanov M, Vasilev EI, Elperin T (2002) Hysteresis Processes in the Regular Reflection ↔ Mach Reflection Transition in Steady Flows. Progress in Aerospace Sciences 38:347–387

Chernity GG (1999) Some Recent Results in Aerodynamic Applications of Flows with Localized Energy Addition. AIAA Paper No. 1999-4819

Chpoun A, Passerel D, Lengrand J-C, Li H, Ben-Dor G, (1994) Mise en Evidence Experimentale et Numerique d'un Phenomene d'Hysteresis lors de la Transition Reflexion de Mach-Reflexion Reguliere. C R Acad Sci Paris 319(2):1447–1453

Chpoun A, Passerel D, Li H, Ben-Dor G (1995) Reconsideration of Oblique Shock Wave Reflection in Steady Flows–Part 1. Experimental Investigation. J. Fluid Mech. 301:19–35

Hornung H, Oertel H, Sandeman R (1979) Transition to Mach Reflection of Shock Waves in Steady and Pseudosteady Flow With and Without Relaxation. J. Fluid Mechanics 90:541–560

Ivanov M, Gimelshein S, Beylich A (1995) Hysteresis Effect in Stationary Reflection of Shock Waves. Physics of Fluids 7: 685–687

Ivanov M, Beylich A, Gimelshein S, Markelov G (1996) Numerical Investigation of Shock Wave Reflection Problems in Steady Flows. The 20th International Symposium on Shock Waves, pp. 471–476

Ivanov M, Klemenkov G, Kudryavtsev A, Nikiforov S, Pavlov A, Fomin, V, Kharitonov A, Khotyanovsky D, Hornung H (1997) Experimental and Numerical Study of the Transition between Regular and Mach Reflections of Shock Waves in Steady Flows. The 21st International Symposium on Shock Waves

Ivanov M, Markelov G, Kudryavtsev A, Gimelshein S (1998) Numerical Analysis of Shock Wave Reflection Transition in Steady Flows. AIAA J. 36(11):2079–2086

Ivanov M, Khotyanovsky D, Kudryavtsev A, Nikiforov S (2001) Experimental Study of 3D Shock Wave Configurations During RR ↔ MR Transition. The 23rd International Symposium on Shock Waves

Ivanov M, Vandromme D, Fomin V, Kudryavtsev A, Hadjadj A, Khotyanovsky D (2001) Transition between Regular and Mach Reflection of Shock Waves: New Numerical and Experimental Results. Shock Waves 11:199–207

Ivanov M, Ben-Dor G, Elperin T, Kudryavtsev A, Khotyanovsky D (2002) The Reflection of Asymmetric Shock Waves in Steady Flows: A numerical investigation. Journal of Fluid Mech. 469:71–87

Khotyanovsky D, Kudryavtsev A, Ivanov M (1999) Numerical Study of the Transition between Steady Regular and Mach Reflection Caused by Freestream Perturbations. The 22nd International Symposium on Shock Waves

Knight D, Kuchinskiy V, Kuranov A, Sheikin E (2002) Aerodynamic Flow Control at High Speed Using Energy Deposition. Fourth Workshop on Magneto- and Plasma Aerodynamics for Aerospace Applications, IVTAN, Moscow, Russia

Kolesnichenko YF, Brovkin VG, Azarova OA, Grudnitsky VG, Lashkov VA, Mashek ICh (2003) MW Energy Deposition for Aerodynamic Application. AIAA 2003-0361

Levin V, Terent'eva L (1993) Supersonic Flow Over a Cone with Heat Release in the Neighborhood of the Apex. Mekhanika Zhidkosti i Gaza 2:110–114

Li H, Chpoun A, Ben-Dor G (1999) Analytical and Experimental Investigation of the Reflection of Asymmetric Shock Waves in Steady Flows. Journal of Fluid Mech. 390:25–43

Molder S (1979) Particular Conditions for the Termination of Regular Reflection of Shock Waves. CASI Trans 25:44–49

Myrabo L, Raizer Y (1994) Laser-induced Air Spike for Advanced Transatmospheric Vehicles. AIAA Paper 1994-2451

Pilyugin N, Talipov R, Khlebnikov, V (1997) Supersonic Flow over the Bodies by the Flow with Physical-Chemical Heterogeneity. Thermophysics of High Temperatures 35:322–336

Riggins D, Nelson H, Johnson E (1999) Blunt Body Wave Drag Reduction Using Focused Energy Deposition. AIAA J. 37(4):460–467

Schmisseur J, Gaitonde D (2001) Numerical Simulation of Mach Reflection in Steady Flows. AIAA Paper 2001-0741

Skews B (1997) Aspect Ratio Effects in Wind Tunnel Studies of Shock Wave Reflection Transition. Shock Waves 7:373–381

Skews B (2000) Three Dimensional Effects in Wind Tunnel Studies of Shock Wave Reflection. J. Fluid Mech. 407:85–104

Toro P, Myrabo L, Nagamatsu, H (1998) Pressure Investigation of the Hypersonic 'Directed Energy Air Spike' Inlet at Mach Number 10 up to 70kW. AIAA Paper 1998-0991

Tretyakov P, Garanin A, Kraynev V, Tupikin A, Yakovlev V (1996) Investigation of Local Laser Energy Release Influence on Supersonic Flow by Methods of Aerophysical Experiments. International Conference on Methods of Aerophysical Research, Novosibirsk, Russia

Von Neumann, J (1963) in Collected Works, Pergamon Press 6:239-299

Yan H, Adelgren R, Boguszko M, Elliott G, Knight D (2003) Laser Energy Deposition in Quiescent Air. AIAA Paper 2003-1051

www.aerosft.com

www.icemcfd.com